J Mater Sci: Mater Electron

Ultrasonication assisted synthesis of nickel decorated poly(diphenylamine) composite based modified electrode for high performance methanol electro oxidation

Veni Keertheeswari Natarajan[1], Suba Lakshmi Madaswamy[1,2], Saikh Mohammad Wabaidur[3], Md Ataul Islam[4], and Ragupathy Dhanusuraman[1,*]

[1] Nano Electrochemistry Lab (NEL), Department of Chemistry, National Institute of Technology Puducherry, Karaikal 609609, India
[2] Department of Chemistry, V.V.Vanniyaperumal College for Women, Virudhunagar 626001, India
[3] Chemistry Department, College of Science, King Saud University, Riyadh 11451, Saudi Arabia
[4] Division of Pharmacy and Optometry, School of Health Science, University of Manchester, Manchester, UK

Received: 27 June 2022
Accepted: 27 September 2022

ABSTRACT

In this present work, a comparatively less expensive and more abundant nickel (Ni) supported on poly(diphenylamine) (PDPA) has been utilized as a potential substitute to noble metal catalyst for methanol oxidation. The hybrid catalyst of nickel over PDPA matrix (Ni@PDPA) was successfully synthesized via ultrasonication method. Average size of nickel catalyst was identified to be 100–200 nm and was analyzed through field emission scanning electron microscopy. The as synthesized Ni@PDPA hybrid catalyst crystalline natures were characterized through X-ray diffraction studies. The nature of bonding was analyzed through Fourier transform-infra red spectroscopy. Ni@PDPA hybrid catalyst gave a peak current density of 1.93 mA/cm^2 at 0.84 V during methanol oxidation reaction. The results obtained proved that Ni@PDPA hybrid catalyst serves to be an efficient electrocatalyst for the application of direct methanol fuel cell.

1 Introduction

The direct methanol fuel cell (DMFC) is a power source that converts methanol chemical energy directly to electricity. There is a great deal toward the study of methanol oxidation. The methanol fuel has numerous benefits, including being lightweight, small in size, long-lasting, and easy to replenish [1]. The commercialization of DMFCs relies on the anode electrocatalyst of low cost and better performance. Among the known electrocatalysts, the adsorption and decomposition of methanol take place by using the criterion catalyst platinum (Pt) which is considered to be exhibiting excellent activity toward

Address correspondence to E-mail: ragu.nitpy@gmail.com; ragu@nitpy.ac.in

https://doi.org/10.1007/s10854-022-09231-4
Published online: 19 October 2022

methanol, whereas Pt has a high price and is highly susceptible to carbon monoxide (CO) toxicity. It is also volatile, has low long-term resilience, and is highly susceptible to CO poisoning [2, 3]. The above demerits can be overruled by the combination of non-noble metal (Ni, Co, Fe, and Mn) which is the most promising candidates having a conducting polymer matrix (polyaniline, poly(diphenylamine), and polypyrrole), i.e., nickel along with the supporting catalysts such as poly(diphenylamine), a suitable substitute for platinum, and used to be a superior catalyst in the field of DMFCs [4]. Nickel is a low-priced metal and earth plenteous catalytic material for DMFC. Under alkaline conditions, nickel-based catalysts have been demonstrated to be the most active, and they remain the most popular catalytic material for DMFC applications [5]. Many of the viable alkaline catalysts for alcohol electro-oxidation comprise precious metals, most commonly platinum or palladium [6, 7]. During electrocatalysis, non-noble metal-based catalysts can stay stable and effective in direct methanol fuel cell. Despite there are several examples of electrocatalytic fuel oxidation using non-precious metal catalysts, further study is required to make these materials compete with their noble metal competitors [8]. Thus, the supporting catalyst material deserves a prominent place in enhancing the electrocatalytic activity in MOR [9–13]. During recent years, conducting polymers such as derivatives of polyaniline (PANI) like poly (2, 5-dimethoxyaniline (PDMA)) and poly(diphenylamine) (PDPA)), polythiophene (PTh), and polypyrrole (Ppy) have been widely used as electrocatalyst for various applications including supercapacitor, biosensor, and electrocatalytic oxidation reaction because of their loftier physicochemical and electrochemical properties [14–20]. Polydiphenylamine (PDPA), a PANI derivative, is an important conducting polymer since it has special properties that are similar to PANI, such as high conductivity, significant electrochemical stability, reasonable price, excellent electrocatalytic activity, and two stable oxidized forms, namely polaronic (diphenylbenzidine cation, $DPSI^{+}$) and bipolaronic (diphenylbenzidine dication, $DPSI^{2+}$) [21–23]. An alternate single and double bonds have made PDPA to form the electron system conjugated. The polaronic and bipolaronic forms of electron flow have strong electrical conductivity and reversible redox activity. Due to its simple synthesis, PDPA has gained a special attention under potentiodynamic conditions and also PDPA matrix is very stable on the electrode surface in aqueous solutions.

Herein, we report ultrasonication-assisted synthesis of nanocomposite of Ni catalyst decorated on PDPA (Ni@PDPA hybrid catalyst) by chemical method using ammonium persulfate as oxidizing agent. The as prepared electrocatalysts were characterized by field emission scanning electron microscopy (FESEM) with energy-dispersive X-ray spectroscopy (EDX), X-ray diffraction (XRD), and Fourier-transform infrared (FT-IR) spectroscopy. Electrochemical work was performed by cyclic voltammetry (CV), impedance spectroscopy (EIS), and chronoamperometry (CA) methods. Because of the synergistic interaction between Ni catalyst and PDPA, the enhanced Ni@PDPA hybrid catalyst exhibits enhanced electrocatalytic activity, stability, and durability in the methanol oxidation reaction.

2 Experimental

2.1 Chemicals and materials

The precursors namely diphenylamine (99%), nickel chloride (99%), ammonium persulfate (98%), hydrazine hydrate (98%), dimethyl formamide (99%), sulfuric acid (98%), sodium hydroxide (97%), ethanol (99%), and methanol (99%) were bought from Merck, India. The chemicals listed in the present experiment is of analytical grade and utilized as received. Deionized water was used for the present experiment. Fluorine-doped tin oxide (FTO) substrate was used as an electrode matrix.

2.2 Instrumentations

Antech ultrasonic cleaner (GT Sonic) was used for the synthesis of PDPA, Ni, and Ni@PDPA hybrid catalyst. For centrifugation, REMI Centrifuge (R-4C) was used. Field emission scanning electron microscopic (FESEM) images were captured through CARL ZEISS (USA) model. The crystalline nature of the synthesized PDPA, Ni, and Ni@PDPA hybrid catalyst was characterized by X-ray diffraction (XRD) with Cu-Kα radiation (Empyrean, Malvern analytical). The molecular vibrational studies are analyzed by Fourier-transform infrared (FT-IR) spectra (Schimadzu IR Affinity model) using KBr pellet technique ranging

from 500 to 4000 cm^{-1}. OrigaLys-OFG500 (Made in France) electrochemical work station was used to perform the electrochemical studies. The three-electrode setup, which includes the working electrode (FTO), reference electrode (Ag/AgCl), and counter-electrode (platinum electrode), was used to investigate electrochemical techniques such as cyclic voltammetry (CV), electrochemical impedance spectroscopy (EIS), and chronopotentiometry (CP).

3 Synthesis method

3.1 Synthesis of PDPA using ultrasonication

Ultrasonication was used to dissolve 40 mM of DPA in 50 ml of 1 M sulfuric acid for 10 min. In a dropwise manner, 50 ml of 20 mM ammonium persulfate was added to the reaction mixture. Ultrasonication is continued for another 10 min after the addition of last drop of APS. Bright green-colored precipitate was then centrifuged for 2 min at 1000 rpm. The precipitate was rinsed with distilled water multiple times. The resulting precipitate was dried and stored at room temperature.

3.2 Synthesis of Ni using ultrasonication

Nickel powders were prepared by reducing nickel chloride in an aqueous solution using hydrazine hydrate as a reducing agent. In 60 mL of distilled water, 0.5 g of nickel chloride ($NiCl_4$ $0.6H_2O$) was dissolved. Solutions were made in a separate beaker by dissolving 1.0 g of NaOH in 20 ml distilled water, and 20 ml of hydrazine hydrate. Aqueous nickel chloride solution was added slowly into it. The resulting solution was now a royal blue color, and it was ultrasonicated again for five minutes and the pH of this solution was found to be 12. Black-colored precipitate of Ni separated out was centrifuged, preserved after being rinsed with distilled water, and dried at room temperature.

3.3 Synthesis of Ni@PDPA hybrid catalyst using Ultrasonication

40 mM diphenyl amine was treated in 50 mL 1 M sulfuric acid, to which 0.1 g Ni was added (previously prepared) and the resultant solution was ultrasonication for 10 min. Dropwise, 50 ml of 20 mM APS was added to the reaction mixture. Bright green-colored precipitate was then centrifuged for 2 min at 1000 rpm. The precipitate was rinsed with distilled water several times before being dried.

3.4 Fabrication of Ni@PDPA hybrid catalyst modified electrode

To remove any debris, the FTO electrodes were first cleaned with distilled water and then rinsed with ethanol. After that, it is kept for drying which serves as bare working electrode for electrochemical workstation. Ni@PDPA hybrid catalyst was fabricated using a solution of DMF / ethanol (50%). The colloidal suspension was mixed well and using a microsyringe, this suspension is drop cast on the surface of FTO and cured at room temperature. In a similar fashion, the other electrodes viz., PDPA and Ni were also fabricated. The fabrication of Ni@PDPA hybrid catalyst toward methanol oxidation is given as a graphical abstract in Fig. 1. Supporting electrolyte in methanol oxidation is the primary factor in the reaction which is given in Eq. 1. Methanol oxidation in alkaline media is a $6e^-$ oxidation that produces CO_2, as illustrated in Eq. 1. Due to the fact that hydroxide ions play in the entire reaction, the pH of the supporting electrolyte is a crucial element in methanol oxidation.

$$\begin{aligned} &CH_3OH + 6OH^- \rightarrow CO_2 + 5H_2O + 6e^- \\ &EO = -0.810 \text{ vs SHE @ pH} = 12 \end{aligned} \quad (1)$$

4 Results and discussions

4.1 Structural investigation

FESEM images of pure PDPA, pure Ni and Ni@PDPA hybrid catalyst are given in Fig. 2. It can be inferred that pure Ni was found to be present as aggregated flakes in Fig. 2(i), while pure PDPA occurs as agglomerated granular structure in Fig. 2(ii). Figure 2(iii) shows the FESEM images of the nanocomposite Ni@PDPA hybrid catalyst showing a heterogeneous morphology in the form of aggregated particles of PDPA decorated by Ni. Figure 2(iv) is the higher magnification image of 2 (iii). It can be depicted that Ni with sizes ranging from 100 to 200 nm on the surface of PDPA. Figure 3 gives the

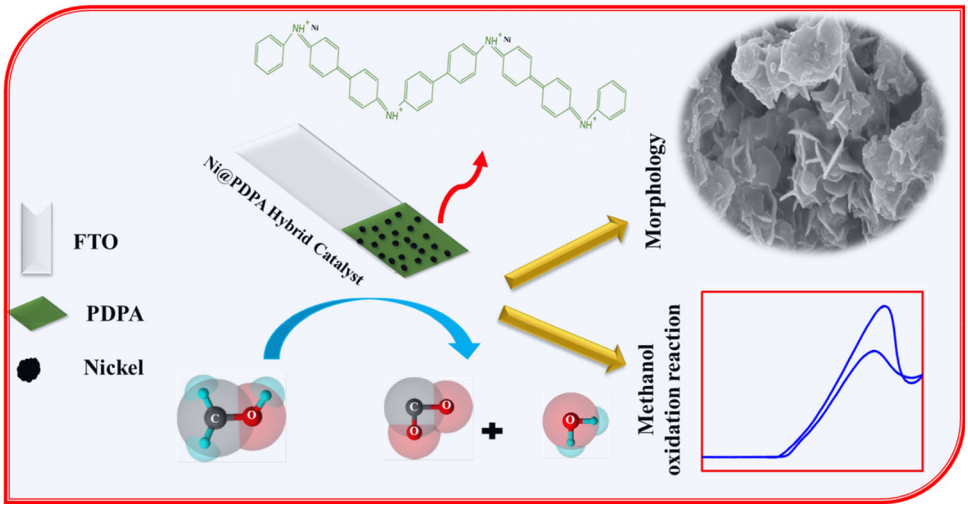

Fig. 1 The scheme of fabrication of Ni@PDPA hybrid catalyst toward methanol oxidation

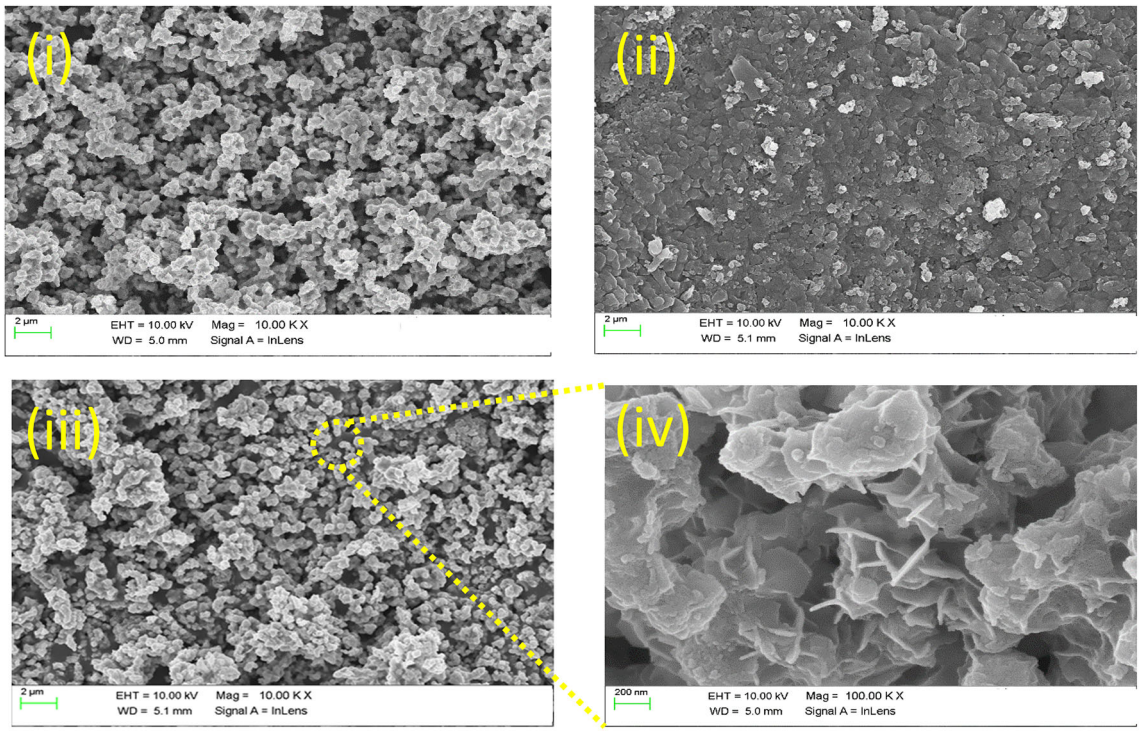

Fig. 2 FESEM images of (i) Ni, (ii) PDPA, (iii) Ni@PDPA hybrid catalyst, (iv) higher magnification image of (iii)

energy-dispersive X-ray (EDX) analysis of Ni@PDPA hybrid catalyst which exhibits the presence of carbon, nitrogen, oxygen, and nickel.

XRD patterns were used to analyze the crystallinity nature of the nanostructured PDPA, Ni, and Ni@PDPA hybrid catalysts which are given in Fig. 4a–c, respectively. In Fig. 4a, PDPA shows a sharp peak at 2θ = 7°,11°, 18°, and 21° which corresponds to the Miller index of (0 2 5), (0 2 3), (0 2 5), and (1 1 0), respectively, shows the presence of PDPA. The crystal growth at a lower 2θ values is due to the effect of ultrasonication which is evident from its XRD patterns [23, 24]. In Fig. 4b, Ni shows a sharp peak at 2θ = 44°, 51°, 76° which corresponds to the Miller index (1 1 1), (2 0 0), and (2 2 0), respectively. Figure 4c depicts the XRD patterns of Ni@PDPA hybrid catalyst authenticates the peaks at 2θ = 7°, 11°, and 18° with a Miller index of (0 2 5), (0 2 3), and (0 2 5), respectively, and 2θ = 44°, 51°, 76° with a Miller index of (0 2 5), (0 2 3), (0 2 5), and (1 1 0),

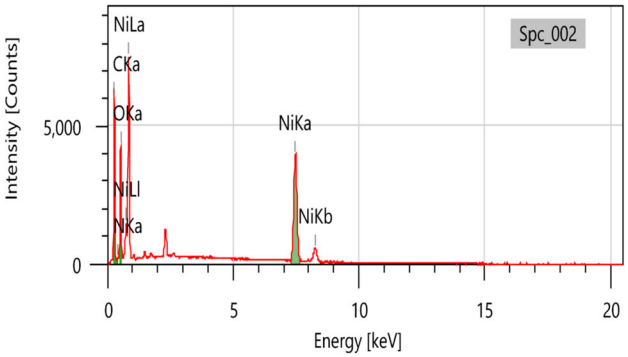

Fig. 3 EDX analysis of Ni@PDPA

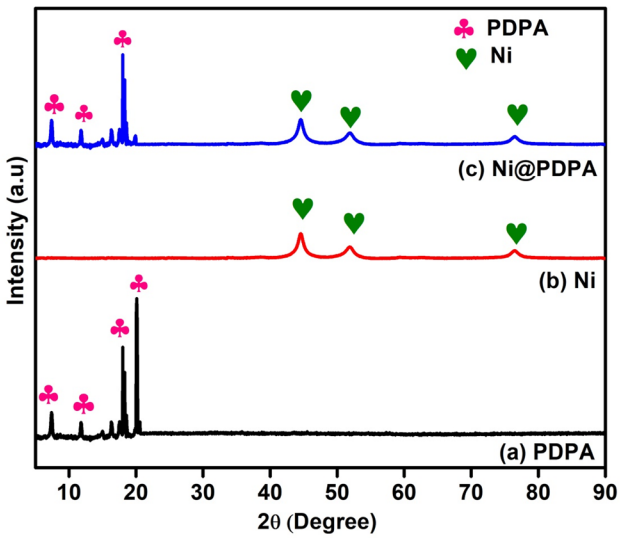

Fig. 4 XRD pattern of **a** PDPA **b** Ni **c** Ni@PDPA hybrid catalyst

respectively, conforms the presence of PDPA and Ni. The values correlated well with JCPDS values bearing the card No 00-047-2216 for PDPA and 01-077-8341 for Ni [25].

The FT-IR spectrum of PDPA, Ni, and Ni@PDPA hybrid catalyst is given in Fig. 5a–c. The spectra were recorded in the mid-infrared region of 500–4000 cm^{-1}. Figure 5a shows the FT-IR spectra of PDPA. The peak of PDPA at 3378 cm^{-1} was attributed to the N–H stretching vibration mode. The quinoid and benzenoid phenyl rings namely C=N and C=C stretching are described by the peaks at 1439 cm^{-1} and 1313 cm^{-1} , respectively, for PDPA. The peak at 1005 cm^{-1} is assigned to secondary aromatic amine C-N modes, while the peak at 865 cm^{-1} is assigned to aromatic C-H out-of-plane bending, respectively. These molecular vibrational studies confirm the formation of PDPA. Figure 5b gives the FT-IR peaks for Ni, which exhibited a peak at

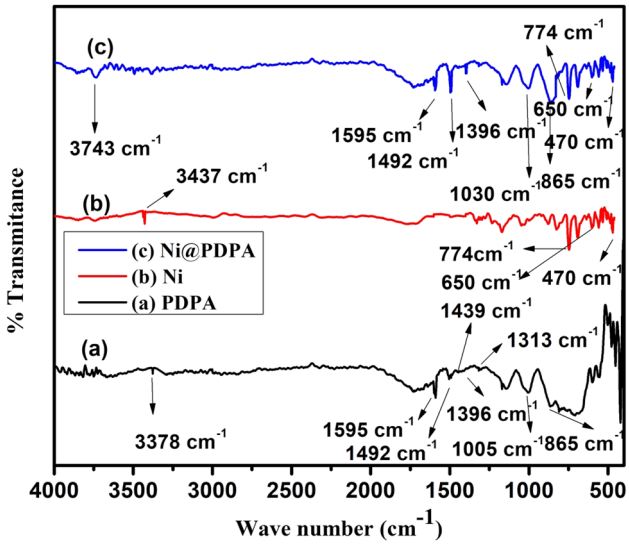

Fig. 5 FT-IR spectra of **a** PDPA **b** Ni **c** Ni@PDPA hybrid catalyst

470 cm^{-1}, 650 cm^{-1}, and 774 cm^{-1} is due to stretching vibrational peak of Ni, and also the peak at 3437 cm^{-1} is due to the presence of moisture (H_2O molecules) [26]. The region around 1400–1500 cm^{-1} is dedicated to the vibrational modes of carbonyl groups, which are absent in the FT-IR spectra of Ni, which suggests the successful synthesis of Ni [27]. Figure 5c gives the FT-IR peaks for Ni@PDPA. The C=C (quinoid) and C=C (benzenoid) vibration peaks of Ni@PDPA hybrid catalyst were observed at 1595 and 1492 cm^{-1} , respectively. The peak intensity of the quinoid stretching vibration is decreased in nanocomposites samples, while the peak intensity of the benzenoid vibration is enhanced; indicating that there is an interaction between Ni and PDPA. FT-IR spectrum of Ni@PDPA hybrid catalyst shows characteristic bands at 1396 cm^{-1} corresponding to C–N stretching characteristic bands of secondary amine. Also the peak at 865 cm^{-1} is assigned to out-of-plane bending of aromatic C–H. A peak at 3378 cm^{-1} is attributed to N–H stretching vibration mode of PDPA is shifted to 3743 cm^{-1} is due to the interaction of Ni with PDPA. The peak intensity of C–N stretching of secondary aromatic amine is increased upon the addition of Ni [28]. Also the peak around 470–770 cm^{-1} confirms the presence of Ni–O stretching and Ni–O–H bending confirming the presence of Ni.

4.2 Electrochemical properties

4.2.1 Cyclic voltammetry (CV) performance of the modified electrode

The CV performance of the modified electrodes viz., bare FTO, PDPA, Ni, and Ni@PDPA hybrid catalyst, was analyzed in 0.1 M KOH solution at the potential range of 0.2 V to 0.6 V at a scan rate of 100 mV s^{-1} is given in Fig. 6. Figure 6a is for bare FTO electrode which shows no characteristic redox peak, (b) PDPA does not exhibits redox peaks in KOH medium, because the behavior of the conducting polymer depends on the pH of the medium [29] (c) Ni shows a redox peaks at 0.496/0.385 V with a current density (0.82 mA/cm.^{2}). This is due to the formation of nickel hydroxide layer over the surface of the nickel electrode when suspended in 0.1 M KOH, which further gets converted to NiO(OH), the equation of which is given below [30]:

$$\mathrm{Ni} + \mathrm{OH}^- \rightarrow \mathrm{Ni(OH)_2} \leftrightarrow \mathrm{NiO(OH)} + \mathrm{H}^+ + \mathrm{e}^- \qquad (2)$$

The electrocatalyst of (a) bare FTO, (b) PDPA, and (c) Ni is given as an insert. Figure 6d shows that Ni@PDPA hybrid catalyst exhibited a significant redox peaks at 0.473/0.305 V with an increased current density (1.8 mA/cm^2) over the entire voltage window, suggesting that Ni@PDPA hybrid catalyst has higher activity for methanol oxidation reaction than PDPA and Ni which follows the equation:

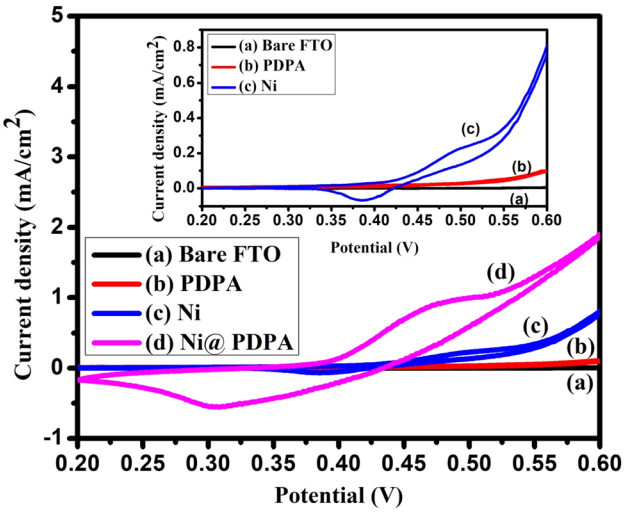

Fig. 6 Cyclic voltametry of **a** Bare FTO **b** PDPA **c** Ni **d** Ni@PDPA hybrid catalyst in 0.1 M KOH. Insert shows (**a**–**c**)

$$\left[(\mathrm{Ni@PDPA})(\mathrm{OH})_2\right] + (\mathrm{OH})^- \leftrightarrow \left[(\mathrm{Ni@PDPA})\,\mathrm{OOH}\right] + \mathrm{H_2O} + \mathrm{e}^- \qquad (3)$$

Thus, the oxidation and reduction of oxyhydroxides and oxides in 0.1 M KOH lead to the formation of sharp peaks as given in Fig. 6. The electrochemical surface area (ECSA) can be calculated using the equation:

$$\mathrm{ECSA} = Q/40 \times \left[(\mathrm{Ni})_{\mathrm{loading}}\right]$$

where Q denotes the charge associated with a reduction of Ni and Ni@PDPA hybrid catalyst and is estimated by the integration of the peak area under the reduction peak of the CVs of Ni and Ni@PDPA hybrid catalyst as given in Fig. 6. The numerical value 40 is the charge required for the reduction in Ni monolayer (μF/cm^2). [$(\mathrm{Ni})_{\mathrm{loading}}$] is the amount of loading of Ni on the electrode surface [31]. It is inferred that Ni and Ni@PDPA hybrid catalyst resulted in the ECSA values of 4.1 m^2/g and 5.2 m^2/g, respectively, which suggests that Ni@PDPA hybrid catalyst exhibited more active cites for MOR when compared to Ni.

4.2.2 EIS studies of the modified electrode

EIS is used to analyze the impedance of the prepared electrocatalyst in 0.1 M KOH alkaline solutions to give semicircular curves sequentially. The smaller semi-circle indicates a faster reaction rate, and EIS is an efficient measurement of charge transfer resistance (R_{ct}). EIS is an important tool for understanding the electrode material's electrical behavior [32, 33]. The EIS performance of modified electrodes viz., bare FTO, PDPA, Ni, and Ni@PDPA hybrid catalyst, was analyzed in 0.1 M KOH and is given in Fig. 7. A semicircular path is obtained for (a) bare FTO electrode indicating the greatest charge transfer resistance at a higher frequency region. The lower frequency semicircles imply a lower charge transfer resistance. The charge transfer resistance follows the order: (a) bare FTO (439 Ω.cm^2), (b) PDPA (271 Ω.cm^2), (c) Ni (213 Ω.cm^2), and (d) Ni@PDPA hybrid catalyst (184 Ω.cm^2). From the above data, it is clear that there is an synergistic interaction between Ni and PDPA, which improves the mobility of electrons and thereby contributing to a better electrochemical oxidation for methanol. The equivalent circuit for

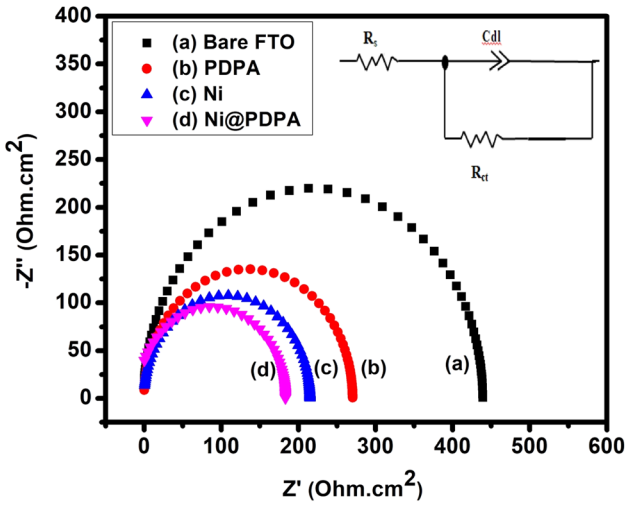

Fig. 7 Nyquist plot of **a** Bare FTO **b** PDPA **c** Ni **d** Ni@PDPA hybrid catalyst in 0.1 M KOH

Ni@PDPA hybrid catalyst is given as an insert in Fig. 7.

4.2.3 *Electrocatalytic activity toward MOR*

Alkaline medium is suitable for MOR reaction for Ni-based catalyst in [34, 35]. Figure 8 depicts the redox peak for the modified electrode PDPA, Ni, and Ni@PDPA hybrid catalyst in 0.1 M KOH at the potential range of 0.3 V to 1.0 V which is kept in 1 M methanol. Figure 8a, b is the CV response for the bare FTO and PDPA with 1 M methanol, where a noticeable change was not inferred, but the response of

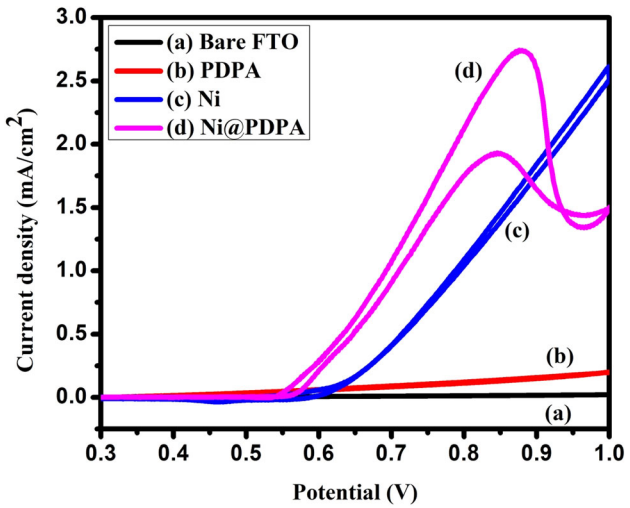

Fig. 8 Cyclic voltammetry of **a** Bare FTO, **b** PDPA, **c** Ni, **d** Ni@PDPA hybrid catalyst in 0.1 M KOH and 0.5 M methanol

PDPA is attributed to the conversion of PDPA to partially oxidized diphenyl benzidine cation (DPSI +). Figure 8c gives the methanol oxidation peak for Ni, which suggests that addition of methanol leads to an increase in the current density (2.6 mA/cm^2) with a pair of redox peaks at 0.5/0.45 V revealing that this electrode is efficient toward methanol oxidation. Ni powders were very sensitive to molecular oxygen in the solution that is adsorbed on the Ni surface and inhibits methanol oxidation reaction. However, quite good catalytic activity was observed for Ni@PDPA hybrid catalyst deposited on FTO substrate as given in Fig. 8d. In both the anodic and cathodic sweeps, distinct pairs of redox peaks are seen for Ni@PDPA hybrid catalyst. Anodic oxidation takes place at 0.84 V with a current density of 1.93 mA/cm^2 with its cathodic counterpart at a potential of 0.86 V and 2.7 mA/cm^2 as its current density. Also, the forward peak current density (I_f) is generally regarded as methanol oxidation on non-poisoned catalysts, while the backward peak current density (I_b) is associated with methanol oxidation on regenerated catalysts (after the removal of the carbonaceous intermediate) [36]. The electrocatalyst Ni@PDPA hybrid catalyst's methanol electro-oxidation was found to be lower in potential when compared to some of the other modified electrodes previously available in the literature and is given in Table. 1, [3, 37, 38] from which it is clear that Ni@PDPA hybrid catalyst has good catalytic activity for oxidation of methanol. This lower potential is due to the synergistic interaction of Ni on PDPA electrocatalyst and also due to depletion of the poisonous species on the catalyst surface is quite efficient. Electrocatalytic performance of Ni@PDPA hybrid catalyst toward methanol oxidation at different scan rates (20 mV/s, 40 mV/s, 60 mV/s, 80 mV/s, and 100 mV/s) in 0.1 M KOH and 1 M methanol is given in Fig. 9. By increasing the scan rate, there is a positive increase in the peak current density for methanol oxidation reaction which suggests that diffusion process predominates during methanol oxidation reaction.

Multiple CV tests (100 cycles) were used to investigate the long-term stability of Ni@PDPA hybrid catalyst and are given in Fig. 10. After 100 cycles, the current density of Ni@PDPA hybrid catalyst decreased to 96% of its initial value suggesting a good cycling stability and better durability for methanol oxidation.

Table 1 Comparison of electrochemical performance of various electrocatalysts toward methanol oxidation reaction

S. No	Electrocatalyst	Methanol oxidation condition	Oxidation potential	Synthesis method	References No
1	PDPA/PTA/Pt	0.5 M methanol in 0.1 M H_2SO_4 with 100 mV/s scan rate	1 V	Electrodeposition	[3]
2	PDMA copolymer DABSA-Pt	1 M methanol and 0.5 M H_2SO_4 with 10 mV/s scan rate	0.9 V	Electrodeposition	[37]
3	Au-mercaptoacetic acid	0.5 M methanol and and 0.5 M H_2SO_4 with 0.5 mV/s scan rate	1.2 V	Electrodeposition	[38]
4	**Ni@PDPA**	**0.1 M KOH and 0.5 M methanol with 100 mV/s scan rate**	**0.84 V**	**Ultrasonication**	**This work**

To highlight our work with other works, bold letters were used

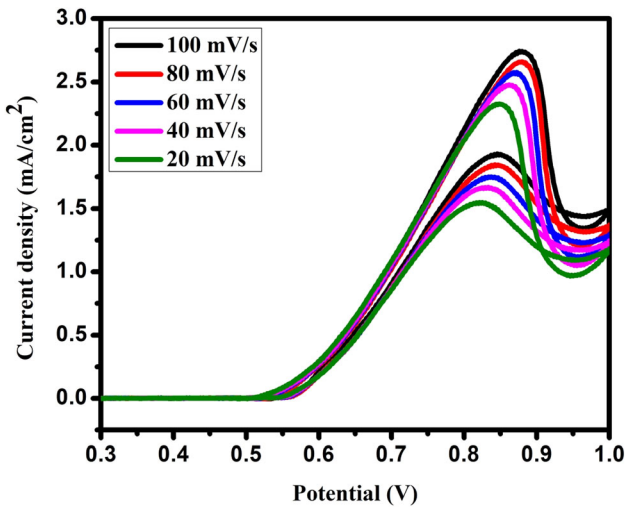

Fig. 9 Cyclic voltammetry curves of Ni@PDPA hybrid catalyst in 0.1 M KOH and 0.5 M methanol at different scan rates

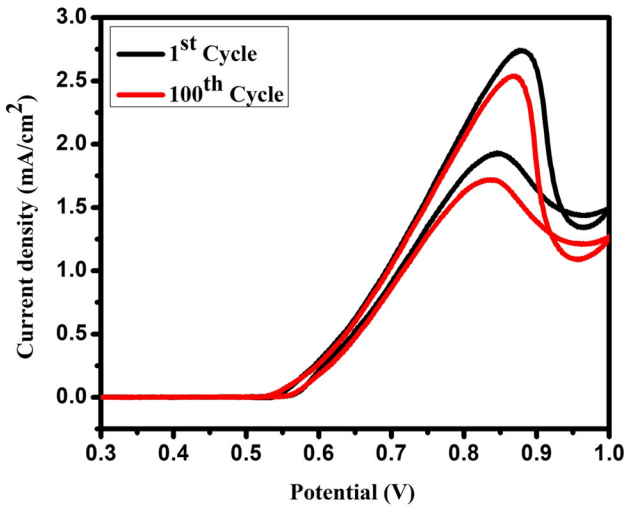

Fig. 10 Cycle stability of Ni@PDPA hybrid catalyst in 0.1 M KOH and 0.5 M methanol

Figure 11(i) represents the performance Ni@PDPA hybrid catalyst toward electro-oxidation of methanol at different concentrations of methanol (1–6 M) in 0.1 M KOH solution. Methanol oxidation current density increases linearly with increase in methanol concentration, i.e., the potential is shifted toward more positive. This is thought to be caused by active site saturation at the electrode's surface. This effect may be noticed because the poisoning rate of Ni rises as the methanol concentration increases, causing the adsorbed intermediates at the Ni surface to be eliminated at higher positive potentials. Also the regression coefficient value (R^2 = 0.9286) suggests that the reaction is diffusion controlled as evident from Fig. 11(ii).

The long-term stability of (a) bare FTO, (b) PDPA, (c) Ni, and (d) Ni@PDPA hybrid catalyst in 0.1 M KOH and 1 M methanol was studied through chronoamperometry (CA) technique. The CA curves were obtained at 0.84 V for 30 min and are given in Fig. 12. As shown in Fig. 12d, Ni@PDPA hybrid catalyst shows better catalytic activity than (b) PDPA and (c) Ni. The current density of (d) Ni@PDPA hybrid catalyst catalysts drastically reduced at first. This could be due to the reactive intermediates produced during oxidation of methanol. At the initial state, the current density was 1.4 mA/cm^2 which is a higher anodic current density than (a) bare FTO (0.28 mA/cm^2), (b) PDPA (0.55 mA/cm^2), and (c) Ni (0.83 mA/cm^2). After the measured time (30 min), still it had higher current density than (b) PDPA and (c) Ni indicating that during methanol electro-oxidation, the Ni@PDPA hybrid catalyst has a better tolerance to the generated intermediates (CO) confirming the increased catalytic performance of

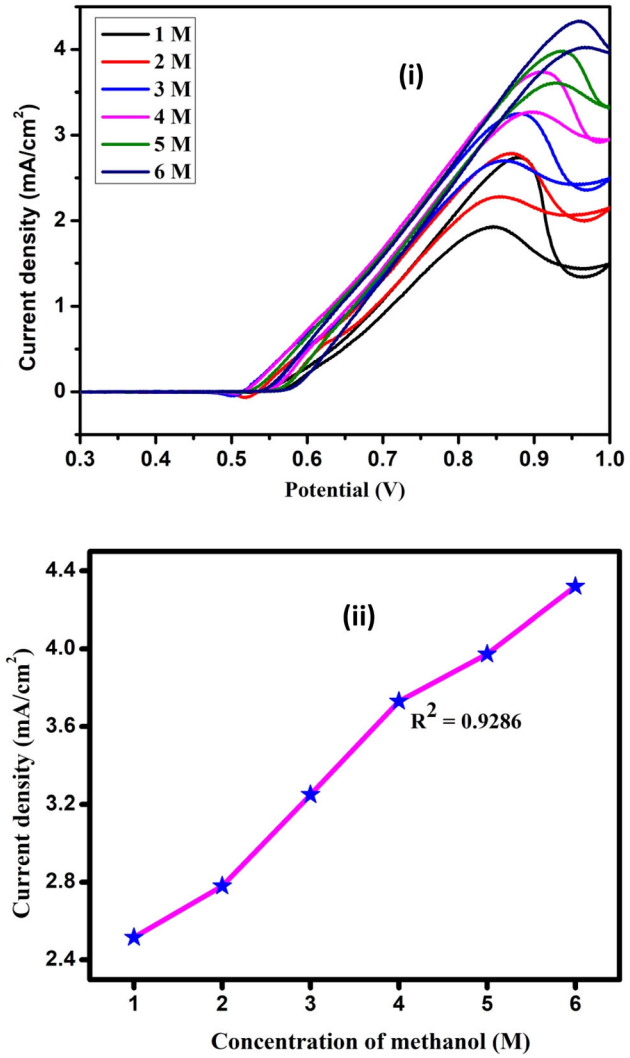

Fig. 11 (i) Cyclic voltammetry curves of Ni@PDPA hybrid catalyst in 0.1 M KOH at different concentrations of methanol and (ii) plot of oxidation peak current density vs. methanol concentration

Ni@PDPA hybrid catalyst compared to (b) PDPA and (c) Ni.

5 Conclusion

In this work, we have produced a unique combination of modified Ni@PDPA hybrid catalyst for methanol oxidation reaction in an alkaline medium using ultrasonication (chemical technique). FESEM and XRD were used to investigate the morphological and structural properties of PDPA, Ni, and Ni@PDPA hybrid catalysts. FESEM images show a heterogeneous morphology in the form of aggregated

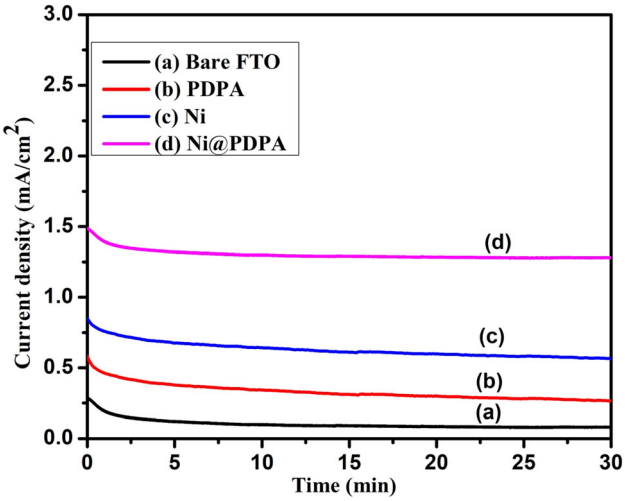

Fig. 12 Chronoamperometric curves of **a** Bare FTO, **b** PDPA, **c** Ni, **d** Ni@PDPA hybrid catalyst in 0.1 M KOH and 0.5 M methanol at 0.84 V

particles of PDPA decorated by Ni. Ni@PDPA hybrid catalyst revealed remarkable characteristics such as increased current density (1.93 mA/cm^2) at a potential of 0.84 V, thereby exhibiting improved electrocatalytic activity and good stability (30 min) when compared to Ni and PDPA. The result implies superior performance of the Ni@PDPA hybrid catalyst for methanol oxidation and as a result, non-precious metal catalysts for alkaline electrochemical applications may be developed in future.

Acknowledgements

Authors are grateful to the Researchers Supporting Project Number (RSP2022R448), King Saud University, Riyadh, Saudi Arabia. Also, the authors would like to thank the basic research support from the National Institute of Technology Puducherry, Karaikal, India.

Author contributions

VKN performed investigation. SLM contributed to writing of the original draft. SMW participated in project administration and funding acquisition. MAI contributed to data interpretation. RD contributed to writing, reviewing, and editing of the manuscript.

Funding

Funding was provided by King Saud University (Grant Number RSP2022R448).

Data availability

The authors confirm that the data supporting the findings of this study are available within the article.

Declarations

Conflict of interest The authors declare that they have no known competing financial interest or personal relationships that could have appeared to influence the work reported in this paper.

References

1. S.L. Madaswamy, A.A. Alothman, M. Al-Anazy, A.A. Ifseisi, K.N. Alqahtani, S.K. Natarajan, D. Ragupathy, Ind. Eng. Chem. Res. **97**, 79–94 (2021). https://doi.org/10.1016/j.jiec.2021.02.008
2. R. Arukula, R.M. Vinothkannan, A.R. Kim, D.J. Yoo, J. Alloys Compd. **771**, 477–488 (2019). https://doi.org/10.1016/j.jallcom.2018.08.303
3. N.V. Keertheeswari, S.L. Madaswamy, S.M. Wabaidur, M.A. Habila, M.M. AlAnazy, R. Dhanusuraman, V.K. Ponnusamy, Prog. Org. Coat. **161**, 106470 (2021). https://doi.org/10.1016/j.porgcoat.2021.106470
4. S.L. Madaswamy, N.V. Keertheeswari, A.A. Alothman, M. Al-Anazy, K.N. Alqahtani, S.M. Wabaidur, R. Dhanusuraman, Advanced industrial and engineering. Polym. Res. **5**, 18–25 (2021). https://doi.org/10.1016/j.aiepr.2021.08.001
5. S.L. Madaswamy, M. Alfakeer, A.A.A. Bahajjaj, M. Ouladsmane, S.M. Wabaidur, C.X. Chen, R. Dhanusuraman, Synth. Met. **281**, 116925 (2021). https://doi.org/10.1016/j.synthmet.2021.116925
6. A. Chen, C. Ostrom, Chem. Rev. **115**, 11999–2044 (2015). https://doi.org/10.1021/acs.chemrev.5b00324
7. N. Kakati, J. Maiti, S.H. Lee, S.H. Jee, B. Viswanathan, Y.S. Yoon, Chem. Rev. **11**, 12397–12429 (2014). https://doi.org/10.1021/cr400389f
8. S.L. Candelaria, N.M. Bedford, T.J. Woehl, N.S. Rentz, A.R. Showalter, S. Pylypenko, B.A. Bunker, S. Lee, B. Reinhart, Y. Ren, S.P. Ertem, ACS Catal. **7**, 365–379 (2017). https://doi.org/10.1021/acscatal.6b02552
9. M.S. Lakshmi, S.M. Wabaidur, Z.A. Alothman, M.R. Johan, V.K. Ponnusamy, R. Dhanusuraman, Int. J. Energy Res. **45**, 8243–8254 (2021). https://doi.org/10.1002/er.5950
10. B. Chokkiah, M. Eswaran, S.M. Wabaidur, Z.A. Alothman, P.C. Tsai, V.K. Ponnusamy, R. Dhanusuraman, Fuel **279**, 118439 (2020). https://doi.org/10.1016/j.fuel.2020.118439
11. X. Yuan, J. Li, C. Zhang, W. Yue, Electrochim. Acta **340**, 135969 (2020). https://doi.org/10.1016/j.electacta.2020.135969
12. M.M. Shahid, A. Pandikumar, A.M. Golsheikh, N.M. Huang, H.N. Lim, RSC Adv. **4**, 62793–62801 (2014). https://doi.org/10.1039/C4RA08952A
13. X. Sun, R. Yan, C. Cheng, B. Jin, Chem. Select. **4**, 9216–9221 (2019). https://doi.org/10.1002/slct.201902255
14. S.L. Madaswamy, N.V. Keertheeswari, R. Dhanusuraman, Conducting polymers: fundamentals, synthesis, properties, and applications, in *Conducting polymers*. CRC Press, Boca Raton, pp. 29–48 (2022)
15. E.K. Joice, S. Rison, K.B. Akshaya, A. Varghese, J. Appl. Electrochem. **49**, 937–947 (2019). https://doi.org/10.1007/s10800-019-01336-9
16. S. Chemchoub, L. Oularbi, A. El Attar, S.A. Younssi, F. Bentiss, C. Jama, M. El Rhazi, Mater. Chem. Phys. **250**, 123009 (2020). https://doi.org/10.1016/j.matchemphys.2020.123009
17. M. Soleimani-Lashkenari, S. Rezaei, J. Fallah, H. Rostami, Synth Met. **235**, 71–79 (2018). https://doi.org/10.1016/j.synthmet.2017.12.001
18. D. Ragupathy, P. Gomathi, S.C. Lee, S.S. Al-Deyab, S.H. Lee, H. Do Ghim, Ind. Eng. Chem. Res. **18**, 1213–1215 (2012). https://doi.org/10.1016/j.jiec.2012.01.032
19. M.S. Lakshmi, S.M. Wabaidur, Z.A. Alothman, D. Ragupathy, Synth. Met. **270**, 116591 (2020). https://doi.org/10.1016/j.synthmet.2020.116591
20. D. Ragupathy, A.I. Gopalan, K.P. Lee, K.M. Manesh, Electrochem. Commun. **10**, 527–530 (2008). https://doi.org/10.1016/j.elecom.2008.01.025
21. S.L. Madaswamy, S.M. Wabaidur, M.R. Khan, S.C. Lee, R. Dhanusuraman, Mac. Res. **29**, 411–417 (2021). https://doi.org/10.1007/s13233-021-9044-1
22. M.S. Lakshmi, E. Muthusankar, S.M. Wabaidur, Z.A. Alothman, V.K. Ponnusamy, D. Ragupathy, Sens. Lett. **18**, 5–11 (2020). https://doi.org/10.1166/sl.2020.4198
23. T.C. Wen, C. Sivakumar, A. Gopalan, Mater. Lett. **54**, 430–441 (2002). https://doi.org/10.1016/S0167-577X(01)00605-X
24. Y.Z. Dong, H.J. Choi, Materials. **12**, 2911 (2019). https://doi.org/10.3390/ma12182911
25. I.S. Pieta, A. Rathi, P. Pieta, R. Nowakowski, M. Hołdynski, M. Pisarek, A. Kaminska, M.B. Gawande, R. Zboril, Appl.

Catal. B **244**, 272–283 (2019). https://doi.org/10.1016/j.apcatb.2018.10.072
26. E. Ramírez-Meneses, I. Betancourt, F. Morales, V. Montiel-Palma, C.C. Villanueva-Alvarado, M.E. Hernández-Rojas, J. Nanoparticle Res. **1**, 743–754 (2011). https://doi.org/10.1007/s11051-010-0039-7
27. S. Sudhasree, A.S. Banu, P. Brindha, G.A. Kurian, Toxicol. Environ. Chem. **96**, 1935–1942 (2014). https://doi.org/10.1080/02772248.2014.923148
28. C. Sathiskumar, C. Alex, N.S. John, Chem. Electron. Chem. **66–98**(7), 1935–1942 (2020). https://doi.org/10.1002/celc.202000176
29. K. Namsheer, C.S. Rout, RSC Adv. **10**, 160–169 (2021). https://doi.org/10.1039/D0RA07800J
30. M. Fleischmann, K. Korinek, D. Pletcher, J. Electroanal. Chem. Interf. Electrochem. **1**, 579–587 (1971)
31. E. Cossar, M.S. Houache, Z. Zhang, E.A. Baranova, J. Electroanal. Chem. **870**, 5617–5622 (2020). https://doi.org/10.1016/j.jelechem.2020.114246
32. A.R. Bredar, A.L. Chown, A.R. Burton, B.H. Farnum, A.C.S. Appl, Energy Mater. **3**, 66–98 (2020). https://doi.org/10.1021/acsaem.9b01965
33. D. Hui, R. Alexandrescu, M. Chipara, I. Morjan, G. Aldica, M.D. Chipara, K.T. Lau, J. Optoelectron. Adv. Mater. **6**, 817–824 (2004)
34. M.A. Rahim, R.A. Hameed, M.W. Khalil, J. Power Sources **134**, 160–169 (2004). https://doi.org/10.1016/j.jpowsour.2004.02.034
35. R.M.A. Tehrani, S.A. Ghani, Fuel Cells **9**, 579–587 (2009). https://doi.org/10.1002/fuce.200800122
36. N. Kakati, J. Maiti, S.H. Jee, S.H. Lee, Y.S. Yoon, J. Alloys Compd. **509**, 5617–5622 (2011). https://doi.org/10.1016/j.jallcom.2011.02.087
37. T.K. Chang, T.C. Wen, Synth Met. **158**, 364–368 (2008). https://doi.org/10.1016/j.synthmet.2008.02.009
38. A. Vulcu, L. Olenic, G. Blanita, C. Berghian-Grosan, Electrochim. Acta. **219**, 630–637 (2016). https://doi.org/10.1016/j.electacta.2016.10.077